Long-term evolution of an AR

L. van Driel-Gesztelyi[1,2]

[1] Konkoly Observatory, Budapest, Pf. 67, H–1525, Hungary
[2] Observatoire de Paris, DASOP, 92195 Meudon Cedex, France
Visiting professor at the University College London

Abstract. I summarize the results of a complex and comprehensive analysis of the evolution of an isolated active region (AR) in the period of July-November 1996. Using SOHO/MDI full-disc magnetic maps, we follow the magnetic evolution of the AR for several months. We extrapolate the photospheric magnetic fields in the linear force-free approximation and match the modelled field lines with the soft X-ray loops observed with the Yohkoh/SXT in order to diagnose the coronal magnetic shear. We find that while the turbulent motions diffuse the flux, the differential rotation, and possibly twisted flux emergence, increase the magnetic shear. Flares are observed during the first three rotations, while CME events (observed by SOHO/EIT and LASCO) originate from this AR from its emergence throughout its decay. Several early CMEs, while none of the late CMEs, are related to flare events above the GOES B1 level. We find that the late CMEs occur when the magnetic shear, after accumulating for four rotations, reaches a high level and saturates. We propose that CME activity serves as a valve through which the AR could get rid of excess shear and helicity.
Furthermore, we study the evolution of the emissivity and heating correlated with magnetic observables of the AR from its birth throughout its decay. Taking one "snapshot" per rotation at each consecutive central meridian passage (CMP) of the AR, outside the time of flares, we analyse multi-wavelength and multi-instrument data obtained from SOHO (MDI and SUMER), Yohkoh (SXT), GOES and 10.7 cm radio data from DRAO, Canada. We find that the magnetic flux density - emitted radiation relations follow a power-law with exponents which appear to depend on the formation temperature (height) of the emission.

Keywords: solar activity, active region evolution. magnetic field, magnetic shear, flare, CME

1. Introduction

During the second half of 1996, solar activity was dominated by a single active region on the southern hemisphere, which was identified as NOAA AR 7978 when it emerged in July. This "last best region" of the cycle (Harvey and Hudson, 1997) provided a rare opportunity for various studies (e.g. (Orlando et al, 1999, Oláh et al, 1999), mainly, because of the lack of other active regions on the Sun its evolution was relatively undisturbed. The evolution of active regions in each and every detail reflects the evolution of the magnetic field which emerges from below, interacts with its magnetic environment, gets dispersed by persistent large-scale flows and more rapidly evolving supergranular and granular convective flows, and furthermore, gets sheared by the differential rotation (van Driel-Gesztelyi, 1998).

Theoretical MHD models have shown that magnetic shear and twist, exceeding a critical threshold, can lead to the destabilization of large-scale coronal arcades (Amari *et al*, 1996; Mikič & Linker, 1997), indicating that they can be considered to be candidates for the initiation of CMEs. In order to test the theoretical predictions we study, for six solar rotations, the occurrence of flare and CME events originating from an AR in the context of the evolution of the coronal magnetic shear.

It is a generally accepted idea that magnetic field plays an important role in heating the solar atmosphere, thus its evolution of an active region must influence the amount of radiation emitted by them. At least two major recent papers dealt with the relations between radiative output and magnetic observables of solar active regions. Fisher et al (1998), using a great combined sample of Yohkoh/SXT images and HSP (Hawaii) vector magnetograms, analysed the relationship between different magnetic observables and soft X-ray emission. They found that the X-ray luminosity is best correlated with the total unsigned magnetic flux of a given AR. Harvey and White (1999) analysed Ca II K images and Kitt Peak magnetograms and found that the Ca II K (residual) intensity is proportional to the half-power of the magnetic flux density. However, none of these important works dealt explicitly with the evolutionary aspect of active regions, what we aim here.

In former papers (van Driel-Gesztelyi et al, 1999a, Mandrini et al, 1999) we studied the long-term evolution of the magnetic non-potentiality combined with flare and CME activity of this AR. In another paper, using multi-wavelength and multi-instrument data, we analysed the evolution of the heating and emissivity of NOAA 7978 from its birth throughout its decay between July and December 1996 (van Driel-Gesztelyi et al, 1999b). Here, summarizing the above former results, I make an attempt to form a global image of long-term active region evolution.

2. Data

During the period of August-October NOAA 7978 was practically the only sizable AR on the Sun, which allowed us the use of one-dimensional datasets like GOES soft X-ray and

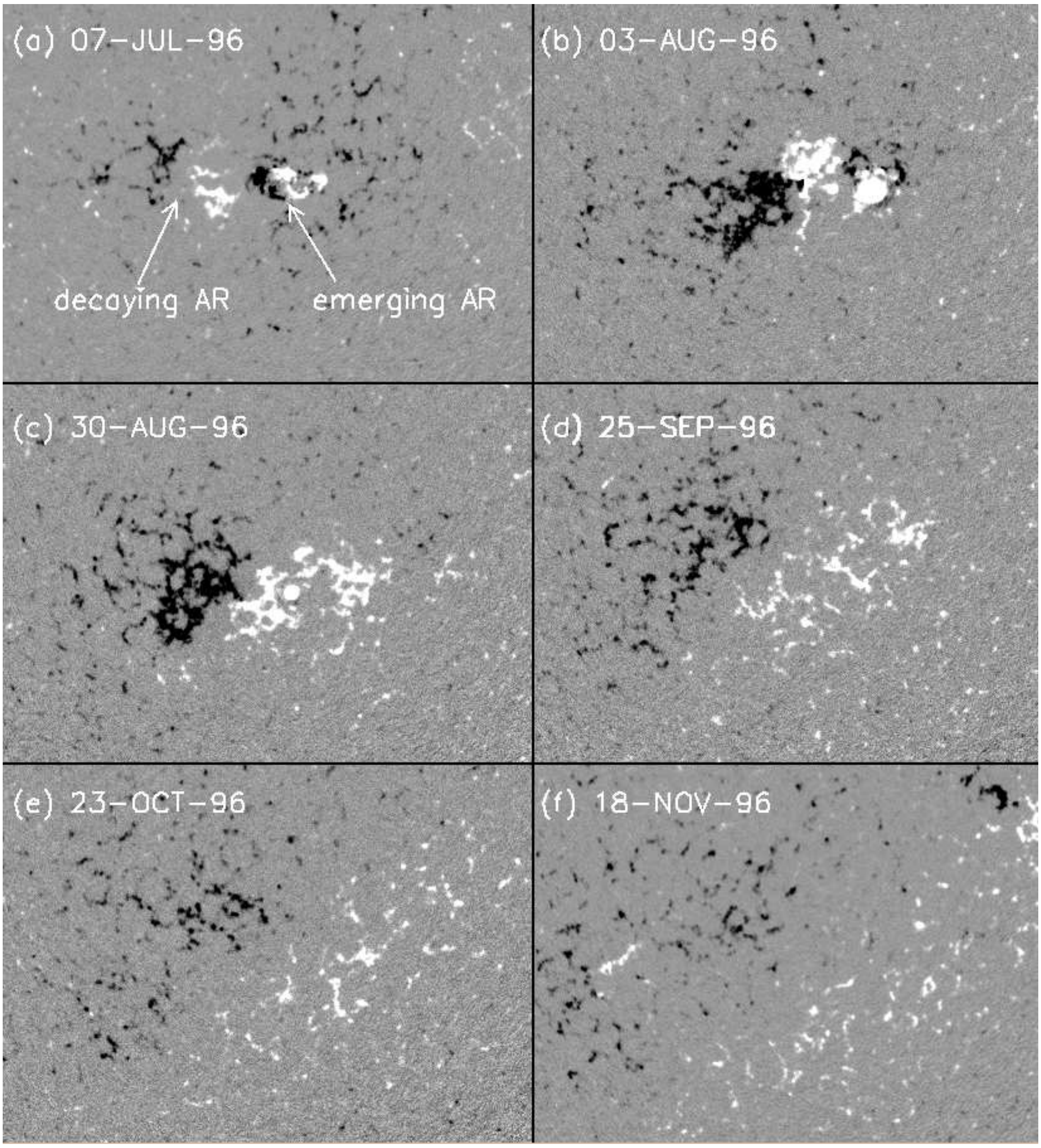

Figure 1: SOHO/MDI magnetic maps show the evolution of the magnetic field distribution of an active region during six months around the time of consecutive central meridian passages (CMPs) of the AR. NOAA AR 7978 was vigorously emerging between 6-10 July, then its decay could be followed for at least six months. Sunspots were present in the AR for two following rotations (CMPs at 2 Aug. and 30 Aug.). The diffusion of the magnetic field is very apparent. The direction of the inversion line is gradually bending about 45°. It is remarkable that any magnetic irregularity in the diffusing bipolar structure is quickly wiped out, presumably by effective flux cancellation processes, the dominant polarity prevails. Note the disappearance of the positive fields of the decaying AR west of the emerging AR between the first and second rotations.

DRAO 10.8 cm radio data besides the two-dimensional SOHO (MDI and SUMER) and Yohkoh/SXT images.

MDI (Michelson Doppler Imager) is one of the twelve experiments on board SOHO, which measures the photospheric manifestation of solar oscillation (Scherrer et al, 1995). Besides the dopplergrams it records the line-of-sight magnetic field, making full-disk magnetograms every 96 minutes. For this analysis we use level-1.5 5-minute averaged data.

SUMER (Solar Ultraviolet Measurements of Emitted Radiation, Wilhelm et al, 1995) performs high-resolution spectral imaging of the Sun at several EUV emission lines. For the present study we use full-disk scans taken in the S VIa 933 Å and SVIb 944 Å lines (T $\approx 2 \times 10^5$ K), which are recorded on different parts of detector A: S VIa on KBr, S VIb on MCP bare. Intensities are calibrated.

The grazing incidence soft X-ray telescope (SXT, Tsuneta et al, 1991) on board of Yohkoh provides images in the 3-60 Å wavelength range. The use of pairs of thin metal filters permits temperature and emission measure analysis of the corona. For this study, we used the thin Al (Al.1) and the aluminum-magnesium sandwich (AlMg) filters.

Geostationary Orbiting Environmental Satellites (GOES) provide soft X-ray irradiance measurements in the 1-8 Å flux range in Wm^{-2}. For our analysis we use low-channel data of the X-ray Sensors (XRS) on board the GOES-9 satellite.

Daily 10.7 cm solar radio flux measurements were recorded at the Dominion Radio Astrophysical Observatory (DRAO) at Pentincton, Canada (Tapping and Charrois, 1994). The daily flux was measured at 17:00, 20:00 and 23:00 UT. The data is given in solar flux units (10^{22} $\mathrm{Wm}^{-2}\mathrm{Hz}^{-1}$) or 10^4 Janskys. Note that both the DRAO and the GOES data were calibrated to 1 AU distance.

3. Magnetic non-potentiality and flare & CME activity of the AR

3.1. Magnetic modelling

We have modelled the field of the AR during six rotations. The modelling has been carried out in the linear force free approach ($\vec{\nabla} \times \vec{B} = \alpha \vec{B}$; α constant) using the extrapolation method described in Démoulin *et al.*, (1997). MDI magnetic field maps at central meridian passage (CMP) have been used as boundary conditions. The free parameter for the model, α, has been chosen in order to fit the shape of the observed SXT loops. We found it impossible to match all the SXT loops at a given time with the same value of α (Figs 2 & 3). In all cases there exists a gradient in the North - South direction. Table 2 shows the evolution of α for six rotations. Keeping the limitations of such diagnostics in mind, we find that AR 7978 emerged in a non-potential state, with the helicity sign corresponding to the southern hemisphere ($\alpha > 0$, see Pevtsov *et al*, 1995). It emerged very close to a pre-existing AR with high helicity in the opposite sense. The latter had vanished by the second rotation. Furthermore, the shear increased from the second to the fourth rotation and then it saturated.

Date 1996	α at the North 10^{-2} Mm^{-1}	α at the South 10^{-2} Mm^{-1}	α of the decaying AR 10^{-2} Mm^{-1}
07 Jul	1.0	–	-5.0
02 Aug	0.75	0.30	–
30 Aug	1.1	0.75	–
25 Sep	1.4	1.00	–
23 Oct	1.4	0.90	–
18 Nov	–	0.90	–

Table 1: Evolution of the shear in the AR – lfff extrapolations.

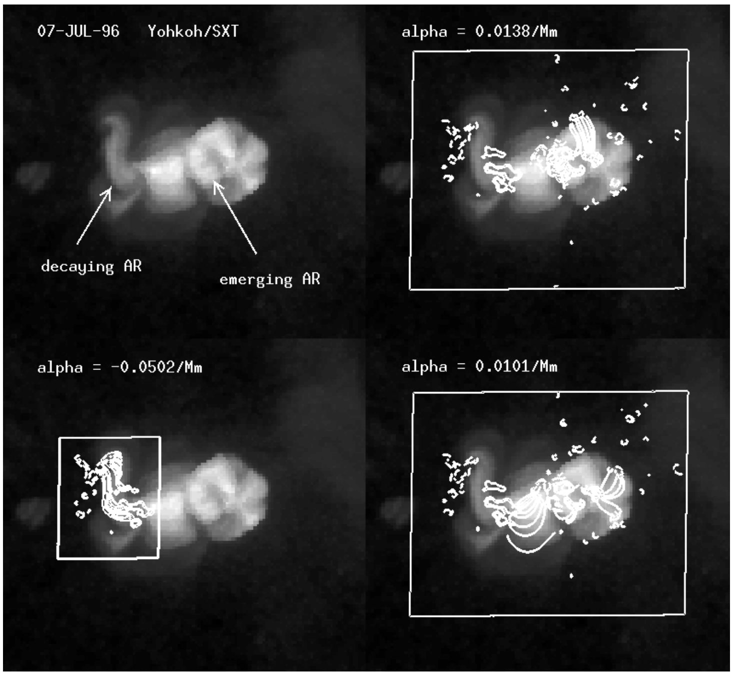

Figure 2: Extrapolated magnetic field lines fitted to coronal loops (SOHO/MDI and Yohkoh/SXT) during the emergence of the AR. The flux appeared already in a non-potential state ($\alpha > 0$). Its interaction with a highly non-potential decaying region ($\alpha < 0$) led to several flares, e.g. the X2.6 flare and CME event on 9 July.

3.2. Flare and CME activity of the AR

Solar activity during the second half of 1996 was dominated by a single active region on the southern hemisphere. The emergence of NOAA AR 7978 was well observed with the SOHO/MDI between 6-10 July 1996, and after that its decay could be followed for at least six more rotations. Table 1 shows that during the vigorous emergence and two following rotations, the AR produced numerous flares (including an X2.6 flare and CME event on July 9, see Dryer *et al.*, 1998) until the disappearance of the main spots by September (see Fig. 1). On the other hand, CME activity, which was at first in several cases related to flare events, continued at a high level for the next three rotations (for an example of the non-flare-related CMEs see e.g van Driel-Gesztelyi *et al*, 1998). The data sources of Table 1 are the GOES X-ray and optical event catalog (http://www.lmsal.com/SXT/operations.html) as well as SOHO/EIT & SOHO/LASCO observations analysed by us (for the LASCO CME list see http://lasco-www.nrl.navy.mil/cmelist.html).

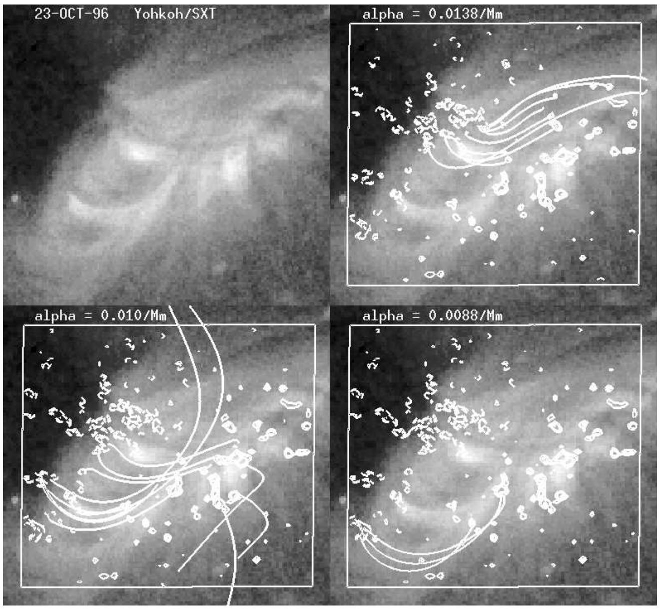

Figure 3: Extrapolated magnetic field lines fitted to coronal loops (SOHO/MDI and Yohkoh/SXT) during the decay phase (fifth rotation) of the AR. Note that α is not uniform and it is high (cf. Table 2).

No. of rot.	Date of CMP 1996	Flares (GOES) X	M	C	B	Type III radio bursts	CME	CME +Flare
1st	07 July	01	02	14	11	2	4	4
2nd	02 Aug.	–	–	–	16	–	8	1
3rd	30 Aug.	–	–	01	08	–	7	2
4th	25 Sep.	–	–	–	–	–	3	–
5th	23 Oct.	–	–	–	–	–	4	–
6th	18 Nov.	–	–	–	–	–	6	–
7th	16 Dec.	–	–	–	–	–	6	–

Table 2: Flare and CME activity in the AR during seven rotations.

4. Emissivity evolution

4.1. Method

Using the images we measured the magnetic flux and the emitted radiation of the active region during the emergence and six more consecutive central meridian passages. We drew the magnetic boundary of the AR "by hand", relying on the detection by the human eye of the steep magnetic field gradient at the boundary using magnetic maps displayed in the same dynamic range (Figs. 1 and 2). We admit that such method brings in some subjective errors, but after carrying out several series of measurements, we did not find greater than about 10 % scatter for the magnetic area and flux. We also used a rectangular area of about 1.6 10^{11} km^2 around the AR for magnetic flux measurements in order to follow the interaction of the newly emerging flux with the pre-existing magnetic environment. This area was always adjusted to the changing solar-terrestrial distance during this half-year period.

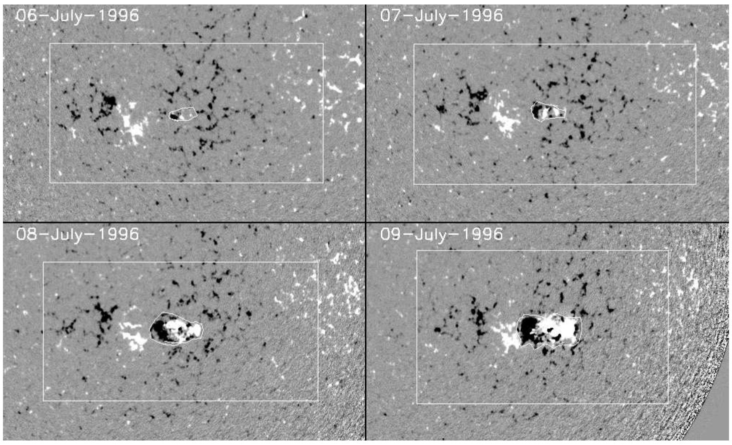

Figure 4: SOHO/MDI magnetic maps show the emergence of NOAA AR 7978, with contours which outline the magnetic area of the growing AR, and another larger area around the AR in which the magnetic flux was measured.

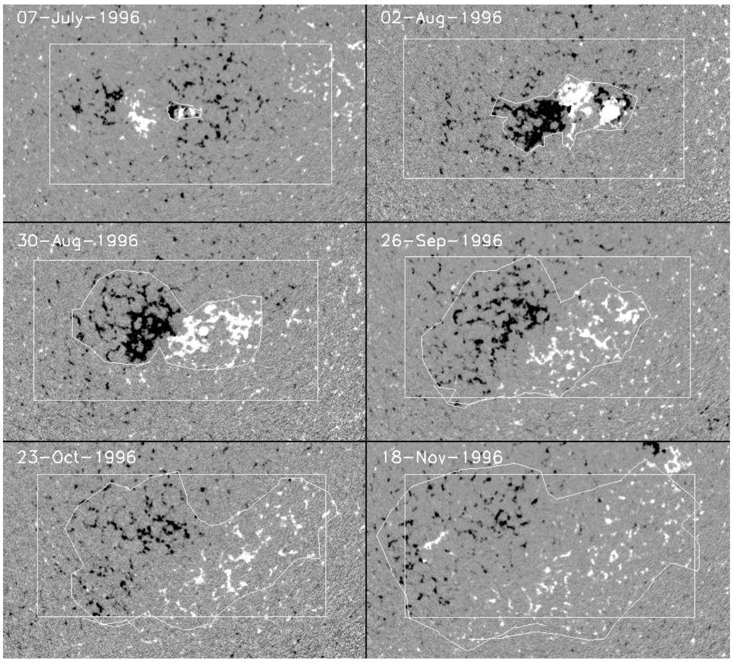

Figure 5: SOHO/MDI magnetic maps show the evolution of NOAA AR 7978 during six solar rotations around the times of central meridian passage. The contours outline the magnetic area of the decaying AR, of which the magnetic flux is getting dispersed. The rectangular area which provided another set of magnetic flux measurements.

The emitted radiation, emission measure and temperature were measured inside the magnetic boundaries of the AR in the images taken closest in time to the central meridian passages.

4.2. Results

We find that the magnetic area of the AR increased roughly linearly at a rate of 1.25 $10^4 \pm 500$ km^{2}sec^{-1}. At the beginning, the X-ray emitting area was larger than the magnetic area, due to interaction of the emerging flux with pre-existing magnetic fields around the AR, i.e. to the formation of bright reconnected loops but it fell behind after the 5th rotation when the magnetic field got very dispersed.

Following the evolution of the magnetic flux in a fixed area of 1.6 10^{11} km^2 containing the growing AR we find an about 20% flux unbalance, due to the fact that the AR emerged in a dominantly negative polarity environment. The total (unsigned) flux inside

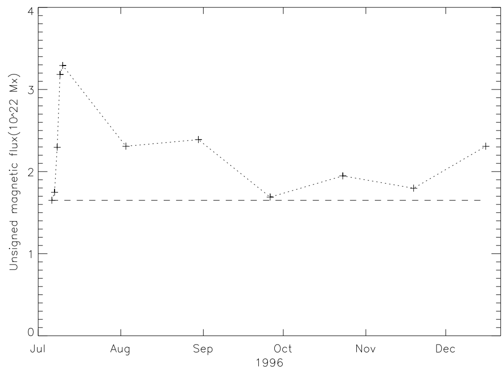

Figure 6: Evolution of the total (unsigned) magnetic flux in a fixed area of 1.6 10^{11} km^2 containing the growing AR. Note that by the fourth rotation the total flux returned to the pre-emergence level.

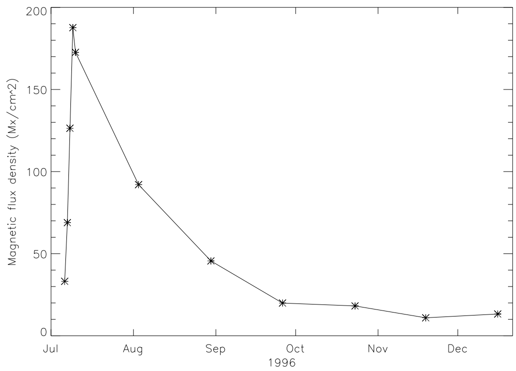

Figure 7: Evolution of the magnetic flux density in the AR versus time. Similarities in the temporal evolution of the magnetic flux density in the AR and the GOES soft X-ray flux suggest physical relationship.

the rectangular area increased two-fold due to the emergence of the AR of 1.5 10^{22} Mx, and it nearly returned to the starting level (i.e. to the total flux in the "box" before the flux emergence) by the fourth rotation (Fig. 3). The increase of the flux in October and after that was due to new flux emergence, i.e. the appearance of minor ARs inside or at the boundary of the decaying AR.

The magnetic flux density (B averaged over the entire AR) reached the highest level (188 Mx cm^{-2}) by the 4th day of the emergence and decreased steadily after that (Fig. 4).

The soft X-ray irradiance (GOES-9) increased steeply during the flux emergence and decreased during the decay phase (outside of flare times). During the evolution process the emissivity did not seem to correlate closely with the area or the total magnetic flux (Fig. 5). The magnetic flux which emerged to form the AR disappeared relatively slowly, followed by an increase after the 4th rotation (Fig. 3), while the SXR emission showed a steep and more steady decrease. On the other hand, intensity, emission measure and temperature shows a better correlation with the magnetic flux density in the AR. We find that the magnetic flux density versus intensity, emission measure and temperature ($\mid B \mid$ vs I, EM and T) of the AR relations follow a power law. These log-log curves show a roughly linear dependence with different slopes. The soft X-ray emission appears to be proportional with the 1.1-1.3 power of the magnetic flux density, while the transition region lines seem to have a power smaller than one (Figs. 6-9).

5. Discussion and conclusions

The flares and CMEs from the early stage of the AR evolution appear to be due to the interaction (cancellation) between the emerging and the pre-existing fields possessing important helicity in the opposite sense. We attribute the shear increase between the

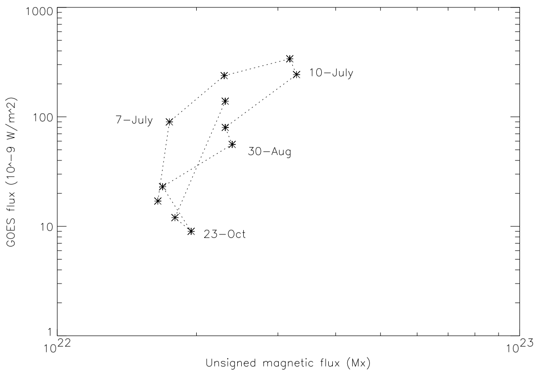

Figure 8: Total magnetic flux over a fixed area of 1.6 10^{11} km^2 around the AR versus the GOES soft X-ray flux indicates a general dependence of the coronal emission on the total magnetic flux. However, roughly the same total flux may relate to very different emission values, depending on the evolutionary stage of the AR.

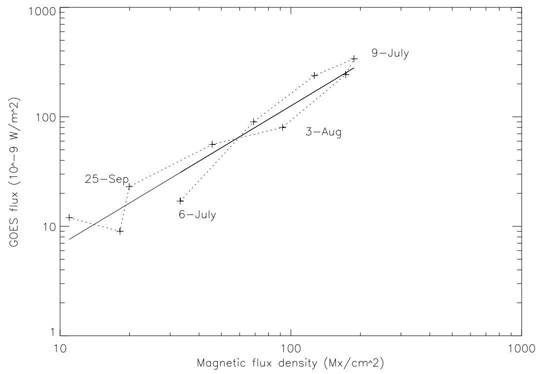

Figure 9: Log-log curve of the magnetic flux density and GOES soft X-ray flux shows a linear function between the two. The X-ray emission appears to be proportional to the 1.3 ± 0.1 power of the magnetic flux density. Note that flux emergence and AR decay may have somewhat different slopes.

second and fourth rotations to twisted flux emergence and shearing by differential rotation. The effect of the differential rotation and even of the emergence of twisted flux did not cease even after four rotations. Still, our results show that the non-potentiality of the AR did not increase any further. We suggest that the shear and helicity which amounted beyond the threshold level was carried away by the CMEs, as suggested by the theory (e.g. Amari *et al*, 1996; Mikič & Linker, 1997).

We find that during the long-term evolution of the AR the magnetic flux density versus intensity, emission measure and temperature ($| B |$ vs I, EM and T) of the AR relations follow a power-law. The log-log curves of these observables are roughly linear with different slopes for coronal and transition line emission. There is even some difference between the slopes of GOES and Yohkoh/SXT data. Though both of these instruments observe in the soft-X-ray domain, the two wavelength ranges are not identical. The GOES/XRS "window" in the soft channel is between 1-8 Å (Hanser and Sellers 1996, Bornmann et al. 1996), while that of Yohkoh/SXT is in the range $\sim 3 - 45$ Å at 1% of peak response (Tsuneta et al. 1991). The passbands of the SXT filters used are about $\sim 3 - 35$ Å (Al.1) and $\sim 3 - 30$ Å (AlMg). The shorter the wavelength, the higher the temperature, thus GOES "sees" the hottest, SXT with the Al.1 filter the coolest coronal plasma (although the Al.1 and AlMg filters have a similar passband). The exponents follow the same trend: we see the highest one in case of GOES (1.3 ± 0.1) and the lowest with the SXT Al.1 filter, though the difference between the two SXT filters may not be significant (1.07 ± 0.09 for the Al.1 filter and 1.13 ± 0.1 for the AlMg filter). When we go to lower temperature and look at the slopes of the $| B |$ versus emission in the SVI lines as observed with SUMER, we find that these transition region lines (T $\approx 2 \times 10^5$ K) have a weaker response to the changing magnetic flux density than the soft X-ray radiation. The scatter is large in the data and there is a difference between the S VIa and the S VIb lines, but the

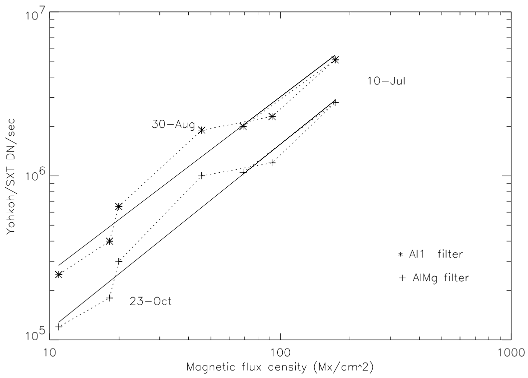

Figure 10: Log-log curves of the magnetic flux density and Yohkoh/SXT DN numbers indicate linearity. The X-ray emission appears to be proportional to the 1.1 ± 0.1 power of the magnetic flux density. Note that this value is somewhat lower than that of the same relation for the GOES flux (cf. Fig. 6 and Table 1).

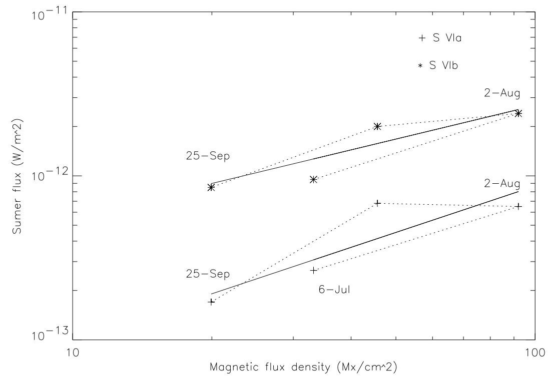

Figure 11: Log-log curves of SUMER S VI line intensities versus magnetic flux density, though the scatter is high for the S VIa line, suggest power laws with exponents of 0.9 ± 0.4 and 0.7 ± 0.2 for these transition region lines – lower values than in the case of the X-ray emission.

exponents are definitely lower than what we found with the SXR radiation. Though the present analysis does not cover a wide range of spectral lines, our results suggest that the exponent in the power law $I \sim \mid B \mid^{exp}$ depends on the formation temperature (or altitude) of the emission. The flattest slope (0.68 ± 0.10) was found with the 10.7 cm radio flux, which has a brightness temperature of $3\ 10^4 K$, but probably at least partially it is of non-thermal origin.

An interesting result is the power-law relation between the magnetic flux density and the soft X-ray temperature: $T \sim \mid B \mid^{0.24 \pm 0.03}$, thus the coronal temperature of the AR is proportional to the quarter power of the magnetic flux density (Fig. 10). The Yohkoh/SXT emission measure seems to have a strong response to the changing magnetic flux density; we found $EM \sim \mid B \mid^{1.3 \pm 0.1}$.

Our findings seem to contradict results by Fisher et al. (1998), who found that the X-ray luminosity of ARs is best correlated with their total unsigned magnetic flux. However, the latter authors dealt with active regions of the same evolutionary stages: all of them were relatively young, and spotless ARs with dispersed magnetic fields were not represented in their sample. Their results simply show that the greater the magnetic flux content of a young AR, the stonger it emits (X-ray) radiation. Studying the evolutionary aspect of emissivity after a given magnetic flux emergence provides an extension of their result. The emissivity of a given total magnetic flux shows dependence on how closely the flux is packed. Also, an evolving active region presents a case when both the total magnetic flux *and* the magnetic flux density are changing.

Recent results by Harvey and White (1999) are in good agreement with our findings and expand the wavelength range studied by us. They found that Ca II K intensity in active regions and plages is proportional to the half-power of the magnetic flux density. The

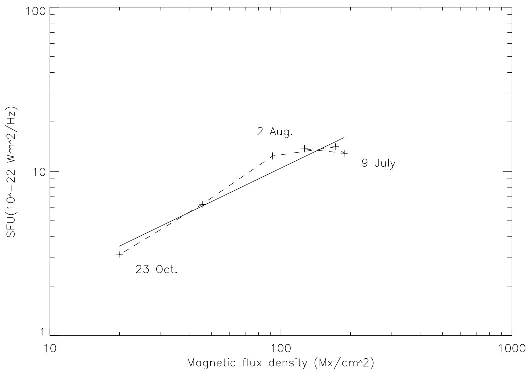

Figure 12: Log-log curve of the residual 10.7 cm radio emission (DRAO) versus magnetic flux density suggests a power law with 0.68 ± 0.10. Note that 10.7 cm radio emission is used as proxi for chromospheric activity, its brightness temperature is about 3 $10^4 K$.

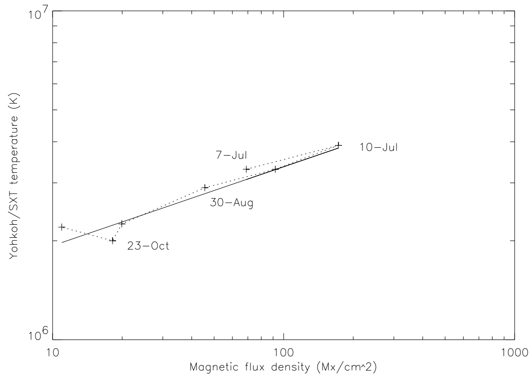

Figure 13: Log-log curve of the Yohkoh/ SXT temperature values versus magnetic flux density indicates a power of 0.24 ± 0.03, i.e. that the coronal temperature of the AR is proportional to the quarter power of the magnetic flux density.

$\mid B \mid$ vs I relation in this cool chromospheric line adds another value to the exponent list given in Table 1, and confirm our suggestion that the exponent depends on the formation temperature (or height in the atmosphere) of the emission.

The results presented above on the long-term evolution of an isolated AR confirmed the introductory sentence, i.e. that the evolution of active regions in each and every detail reflects the evolution of the magnetic field. We have already learned a lot about this AR, but there are still several unanswered questions. We saw that non-potentiality evolves in the active region and that it is related to its flare and CME activity. However, it is not yet explored how much is the contribution of the differential rotation in building up the observed shear and how much can be attributed to a continuing emergence of the twisted flux tube, which formed the AR. As for the emissivity evolution, the wavelength range of the emissivity measurements clearly need to be extended towards the chromospheric and transition-region lines, and the physics behind the discovered power-law dependences betwwen the magnetic flux density and other observables should be explored. The Sun provided us with an almost perfect subject for such evolutionary oriented studies, thus we should make the most of it.

Acknowledgements

I thank the organizers of the meeting for the wonderful "eclipse experience", a mixture of science, enchantment and fun. I thank all my collaborators, B. Thompson, C.H. Mandrini, P. Démoulin, S. Orlando, S. Plunkett, C. Bocchialini, K. Oláh, Zs. Kővári, G. Aulanier, C. DeForest, B. Schmieder, J. Khan and A. Fludra, who helped to realize this ambitious and diverse project, the Yohkoh Team and the MSSL YDAC for the Yohkoh/SXT data, and the SOHO/MDI consortium for the magnetograms. I acknowledge the usefulness of the

Instrument	Temperature	Exponent
GOES 1-8 Å soft X-rays	5-6 10^6 K	1.3 ± 0.1
Yohkoh/SXT 3-35 Å	2-4 10^6 K	1.1 ± 0.1
SUMER S VIa	2 10^5 K	0.94 ± 0.36
SUMER S VIb	2 10^5 K	0.68 ± 0.24
DRAO 10.7 cm radio	3 10^4 K	0.68 ± 0.10

Table 3: Exponents of the power-law describing the magnetic flux density – intensity relations.

Parameter	Exponent
Yohkoh/SXT emission measure	1.32 ± 0.13
Yohkoh/SXT temperature	0.24 ± 0.03

Table 4: Exponents of the power-law describing the magnetic flux density – emission measure and temperature relations.

2nd SOHO/Yohkoh CDAW held at Orsay, France, initiating this project. I acknowledge the Hungarian Government grants OTKA T-026165 and AKP 97-58 2,2.

References

Amari, T., Luciani, J.F., Aly, J.J., and Tagger, M.: 1996, ApJ, 466, L39.

Bornmann, P.L., Speich, D., Hirman, J., Matheson, L., Grubb, R., Garcia, H., Viereck, R., 1996, in Edward R. Washwell (ed.) "GOES-8 and Beyond", Proc. SPIE Vol. 2812, p. 291.

Démoulin, P., Bagalá, L.G. Mandrini, C.H., Hénoux, J.C., and Rovira, M.G.: 1997, A&A, 325, 305.

Dryer, M. and 23 co-authors: 1998, Solar Phys., 181, 159.

Fisher G.H, Longcope D.W., Metcalf T.R., Pevtsov A.A.: 1998, Ap.J., 508, 885.

Hanser, F.A., Sellers, F.B., 1996, in Edward R. Washwell (ed.) "GOES-8 and Beyond", Proc. SPIE Vol. 2812, p. 344.

Harvey, K.L., Hudson. H.S., 1997, in T. Watanabe, T. Kosugi, A.C. Sterling (eds.): "Observational Plasma Astrophysics: Five Years of Yohkoh and Beyond", Kluwer, 315.

Harvey, K.L., White, O.R., 1999, ApJ., 515, 812.

Mandrini, C.H., van Driel-Gesztelyi, L., Thompson, B., Plunkett, S., Démoulin, P., Aulanier, G., 1999, Intern. Geophys., in press

Mikič, Z. and Linker, J.A.: 1997, in "Coronal Mass Ejections", Geophysical Monograph 99, American Geophys. Union. 57.

Oláh, K., van Driel-Gesztelyi, L., Kővári, Zs., Bartus, J.: 1999, Astron. Astrophys. 344, 163.

Orlando, S., Khan, J., van Driel-Gesztelyi L., Thompson, B., Fludra, A., Foing, B., Adv. Space Res., in press

Pevtsov, A.A., Canfield, R.C., and Metcalf, T.R.: 1995, ApJ, 440, L109.

Scherrer, P.H., and 12 co-authors: 1995, Solar Phys. 162, 129.

Tapping, K.F., Charrois D.P., 1994, Solar Phys., 150, 305.

Tsuneta, S., and 12 co-authors: 1991, Solar Phys. 136, 37.

van Driel-Gesztelyi L.: 1998, in C. Alissandrakis and B. Schmieder (eds.) "Three Dimensional Structure of Solar Active Regions", ASP Conf. Ser., 155, 202.

van Driel-Gesztelyi L., Schmieder B., Aulanier, G., Démoulin, P., Martens, P.C.H., Zarro, D., De Forest C., Thompson B., Saint Cyr, C., Kucera T., Burkepile, J.T., White, O.R., Hanaoka, Y., and Nitta, N.: 1998, in D. Webb, D. Rust and B. Schmieder (eds.) "New Perspectives on Solar Prominences", Proc. IAU Coll. 167, ASP Conf. Ser., 150, 366.

van Driel-Gesztelyi L., Mandrini, C.H., Thompson, B., Plunkett, S., Aulanier, G., Démoulin, P., Schmieder, B., and DeForest, C.: 1999, Proc. 3rd ASPE, ASP Conf. Ser., 184, 302.

van Driel-Gesztelyi L., Thompson B., Démoulin, P., Orlando, S., Bocchialini K., Oláh K., Kővári, Z., DeForest, C., Khan J., Fludra A., and Mandrini C.: 1999, "Long-term evolution of the emissivity and heating in a solar active region" Proc. SOHO-8, ESA Publ. SP-446, 663.

Wilhelm, K., and 15 co-authors: 1995, Solar Phys. 162, 189.

Discussion

S. Antiochos: Does the decrease in X-ray emission with the corresponding increase in area in agree with the $I \sim L^{-2}$ result found by Pascal?

L. van Driel: The first rough calculations show that the two results are compatible. We are presently working on a more precise answer.

S. Antiochos: Was there a change in the speed of the CMEs during the evolution of the AR?

L. van Driel: During the flux emergence phase several of the CMEs which originated from this AR were fast flare-related ones , while after the disappearance of the sunspots they were mainly related to filament eruption, thus they belonged to the slow CME category. Like this we can say that in general the speed of the CMEs decreased during the long-term evolution of the AR.

S. Solanki: How large was the spatial box used to determine the total magnetic flux?

L. van Driel: The area of the spatial box was 1.6×10^{11} km^2.

S. Solanki: How does the presence of an older active region influence the estimate of the change in flux of the newly emerged active region?

L. van Driel: We see that the positive (leading) magnetic polarity of the older active region disappeared by the second rotation presumably by flux cancellation. The counterpart of the cancelling positive polarity had to mainly belong to the negative (following) polarity of the new emerging active region. Thus, the evolution of the magnetic flux of the newly emerged active region can not be regarded undisturbed at the beginning.

K. Oláh: The shape of the flux variation curve of the active region reminds me to the shape of a stellar flare though in a much longer time scale. Do you see any possible correlation between this shape and the fact that the number of flares were also decreasing as the active region decayed? Could overlapping flare events result in this kind of behaviour?

L. van Driel: The total emitted flux of the active region carries the combined effects of flaring and heating defined by the scaling laws. The remark on the flare-like shape of the flux versus time is an interesting observation and deserves further consideration.